An overview of oxidation in hybrid and glass-based protective coatings for thermoelectric materials for medium-temperature range applications.

F. D'Isanto[1], F. Smeacetto[1], M. J. Reece.[2] and M. Salvo[1*]*

[1]Department of Applied Science and Technology, Politecnico di Torino, Corso Duca degli Abruzzi 24, 10129 Torino, Italy.

[2]School of Engineering & Materials Science and Nanoforce Technology Ltd., Queen Mary University of London, Mile End Road, London E1 4NS, United Kingdom.

*corresponding author: fabiana.disanto@polito.it

Abstract

Several oxidation protective coatings, both glass-based and ceramic/polymer hybrid coatings, for p- and n-type thermoelectrics were designed at the Politecnico di Torino in recent years, and they were characterised and tested under relevant conditions. The "glass-ceramic route" to obtain a thermo-mechanical compatible and high-temperature resistant coated thermoelectric is discussed with some

examples. Oxidation tests demonstrated the effectiveness of the coatings for the protection of both n- and p-type thermoelectrics.

Keywords: Oxidation protective coatings, Glass-ceramics, Thermoelectrics

1. Introduction

The increasing amounts of electricity are consumed in everyday life, its high cost and the environmental impact of fossil-fuels are guiding research towards alternative energy sources and represent one of the main challenges of the 21st century [1]. The need for sustainable and renewable energy is driving research on the development of new thermoelectric materials (TEs) with exceptional properties such as low thermal conductivity, high electrical conductivity and a large Seebeck coefficient, that are able to more efficiently generate electricity from waste heat [2,3].

A crucial issue in the application of thermoelectric substrates in waste heat recovery is their stability and oxidation resistance over time at high temperatures. Most of the high-performance TEs, such as tellurides and silicides, are oxidised at high temperature in air. In particular, some MnSi-based thermoelectric devices are used at relatively low temperatures (<500°C) to avoid this degradation [4,5]. However, if they could be used at higher temperatures, their efficiency would increase. Some attempts to solve this critical aspect, concern their full encapsulation within stainless-steel containers, in vacuum or filled with an inert atmosphere [6], or with a silica aerogel [7], but this increases considerably the cost of the devices. Different metallic coatings have been investigated [8–12], but their high electrical conductivity resulted in a lower heat to electricity conversion efficiency. Whatever the coating, it should meet the following requirements: (1) chemical stability against TE materials, (2) thermal stability at operating temperatures, (3) CTE matching with TE material, where the interface should possess good compatibility, withstand stress during thermal cycling, and (4) have no significant effect on system performance [13].

Glass-ceramic and glass-based coatings are potentially optimal candidates for protecting thermoelectrics against oxidation. Firstly, they soften and flow above their glass softening temperature (Ts). Furthermore, they are easy to manufacture, and thermally stable with low electrical and thermal conductivity thanks to the versatility of their compositions and properties. They are excellent candidate materials as low-cost protective coatings. In fact, some of their characteristic properties can be tailored to make them suitable for coating different types of substrates and to satisfy the requirements in terms of thermo-chemical stability and thermo-mechanical compatibility with other materials. In particular, the coefficient of thermal expansion (CTE) must be as close as possible to that of the materials to be coated, thus avoiding residual stresses at the thermoelectric/coating interface. Since the composition of the original glass influences the properties of the glass-ceramic obtained after a sinter-crystallization heat treatment, it is important to know the effect that the different constituent oxides have on the amorphous network and on the crystalline phases formed during the devitrification process, thus predicting some thermal (glass transition temperature, Tg, softening point, Tsoft, melting), functional and thermo-mechanical (CTE) properties [14].

There is a growing body of literature that recognises the importance of glass-based oxidation protective coatings for both n- and p-type thermoelectric devices [4,15–17]. In this paper a short overview of different oxidation protective coatings is presented, discussing a different type of coating for each thermoelectric studied: magnesium silicide-based material (Sb-doped $Mg_2(Si,Sn)$, $Mg_2Si_{0.487}Sn_{0.5}Sb_{0.013}$) and titanium suboxide (TiO_{2-x}) as n-type TE; higher manganese silicide, (HMS, $MnSi_{1.74}$) and Zn-doped Tetrahedrite (Zn-doped THD, $Cu_{11.5}Zn_{0.5}Sb_4S_{13}$) as p-type TE.

2. Materials and methods

2.1 TE substrates synthesis

The thermoelectric powders of Sb-doped $Mg_2(Si,Sn)$, HMS and Zn-doped THD were synthesized by a high-temperature calcination method and densified using a spark plasma sintering (SPS) furnace

(HPD25/1, FCT Systeme GmbH) with different sintering conditions depending on the type of thermoelectric substrate:

- 720°C/50 MPa/3 min for magnesium silicide based thermoelectric [18]
- 1000°C/50MPa/3 min for higher manganese silicide [4]
- 400°C/50 MPa/5 min for Zn-doped Tetrahedrite[19]

On the other hand, TiO_{2-x} samples were synthesize starting from TiO_2 and TiC powders and sintering at 1300°C under flowing N_2, using a heating rate of 5 °C/min and with a dwell time of 2 h. More details are reported in ref.[20].

2.2 Glass-based and hybrid oxidation protective coatings

Table I presents an overview of some original glass compositions, designed and characterised at the Politecnico di Torino with the aim of developing oxidation protective coatings for TEs. The different glass compositions ranges were selected with the help of the Sciglass 6.6 software database (AKos GmbH, Germany) and modifying the glass composition based on the properties required for the coatings. The main criteria for the selection of glass-based coatings were the compatibility between the CTE of the coating and the thermoelectric substrate as well as the coatings' glass transition temperature (*T*g) and softening temperature (*T*s).

All of the glasses ("parent glasses") were prepared by weighing and mixing the starting precursors (oxides or carbonates) according to the glass composition reported in Table I. The raw materials were mixed and were subsequently melted at high temperature in a chamber furnace in air, in platinum-rhodium crucibles (Table I). The parent glasses were obtained by melt-quenching by casting onto a brass substrate, which was then ground and sieved into particle size ≤ 38 μm. All the powder glasses were thermally characterised by means of hot stage microscopy (HSM), and differential thermal analysis (DTA).

The coatings were deposited using the slurry method: a slurry composed of ethanol (30 wt.%) and glass powder (70 wt.%) was manually deposited with a spatula onto the thermoelectric substrate and then subjected to selected thermal treatment, based on the results obtained from the thermal analyses (HSM and DTA) performed on the glass powders. All of the heat treatments were carried out in a tubular furnace under a continuous flowing Ar, following the deposition conditions reported in Table I.

The coefficient of thermal expansion (CTE) and the dilatometric softening point of the glass-based coatings were measured (before and after the deposition heat-treatment) using a dilatometer (DIL402PC, Netzsch, Selb, Germany).

Since a glass-ceramic coating would require a deposition temperature too high for the Zn-doped Tetrahedrite, a commercial hybrid water-based resin purchased from AREMCO SCIENTIFIC COMPANY (Los Angeles, USA) and named Corr-Paint CP4040 was tested. It is characterised by having a low curing temperature (250 °C for 45 minutes) and a nominal temperature resistance of up to 590°C, and the composition is reported in Table I. It was applied on the TE substrate using a foam brush and subsequently cured under flowing Ar in a tubular furnace following the deposition conditions reported in Table I. In order to demonstrate the effectiveness of these new innovative coatings against oxidation, coated and uncoated samples were subjected to different oxidation/cycling tests, under the conditions reported in Table I.

Field emission scanning electron microscope (FE-SEM, Merlin electron microscope, ZEISS, Oberkochen, Germany) and energy dispersive X-ray spectroscopy (EDS, Zeiss Supra TM 40, Oberkochen, Germany) were used to morphologically and chemically characterise the coated and uncoated samples before and after oxidation/cycling tests. X-ray diffraction (XRD) analysis was performed using an X'Pert Pro MRD diffractometer with Cu Kα radiation, with the aid of the X-Pert HighScore software. The crystalline phases were identified with the JCPDS data base provided by ICDD (International Centre for Diffraction Data, Newton Square, Pennsylvania, USA). Furthermore,

some samples were analysed by means of a transmission electron microscope (TEM) JEOL 2100F UHR, equipped with a Schottky field emission gun. Images were taken in bright field imaging mode, while the selected area electron diffraction technique (SAED) was used for the investigation of the reciprocal space. EDS spectrometry was carried out to analyse the elemental composition of the samples, employing an Oxford Instruments SDD detector Xmax80. The samples were prepared by mechanical pre-thinning and ion milling using a Gatan PIPS model 691[20].

Compositional changes in both of the p-type thermoelectrics and the coatings are reviewed and discussed with respect to the electrical properties of the uncoated and coated samples before and after thermal cycling or oxidation treatment. The Seebeck coefficient and electrical resistivity were measured in vacuum (ZEM-3, Ulvac Technologies, Inc; Methuen, Massachusetts, USA). In order to calculate the figure of merit of HMS samples, the thermal conductivity (k) was determined using the equation $k = \lambda \cdot Cp \cdot d$, where λ is the thermal diffusivity, Cp is the heat specific and d the density. The thermal diffusivity was measured using a laser-flash method in a flowing Ar atmosphere (LFA- 457 MicroFlash, Netzsch, Selb, Germany); the specific heat capacity was calculated using the Dulong-Petit law to avoid the large uncertainty in the differential scanning calorimetry method, and the density was obtained using the Archimede's method. For all the electrical measurements, the outer layers of both coated and uncoated samples were removed using a sandpaper to allow electrical contacts to take place.

Table I. Summary of glass-based oxidation protective coatings for Sb doped $Mg_2(Si,Sn)$, TiO_{2-x} and HMS thermoelectrics: composition, thermal and thermo-mechanical properties, main crystalline phases, deposition thermal treatment, oxidation/cycling test parameters. Composition and heat-treatment of a commercial hybrid resin used to protect Zn-doped THD are also illustrated (α= coefficient of thermal expansion; Tg= glass transition temperature; Td= softening dilatometric temperature).

TE material/ CTE (α)	Oxidation protective coatings																		
	Glass-based coatings																		
	Parent glass											Glass/ Glass-ceramic after deposition thermal treatment							
n-type	Acronym	Composition (wt%)							Processing (°C)	CTE $\cdot 10^{-6}$ °C^{-1}	Tg (°C)	Ts (°C)	CTE $\cdot 10^{-6}$ °C^{-1}	Tg (°C)	Ts (°C)	Deposition thermal treatment: temperature (°C), time (h),Ar flow	Main crystalline phases	Oxidation/cycling test	Ref
		SiO_2	K_2O	Na_2O	CaO	MgO	Al_2O_3	B_2O_3											
Sb doped $Mg_2(Si,Sn)$ $[Mg_2Si_{0.487}Sn_{0.5}Sb_{0.013}]$ $\alpha \approx 17.6 \cdot 10^{-6}$ °C^{-1}	M1	49.26	25.86	14.78	4.31	2.71	3.08	-	1200°C for 1h + 1250 for 30 minutes, air	17	-	401	19.2	-	454	650°C for 1h	$Ca_9Al_6O_{18}$ K_2AlSiO_4	-	
	M2	51.05	22.56	11.7	7.06	4.44	3.18	-		15.8	468	497	18.5	453	705	650°C for 1h	$Ca_9Al_6O_{18}$ K_2AlSiO_4	-	
	M3	44.05	24.07	13.63	3.41	1.47	3.03	10.33		16.8	-	429	17	409	452	550°C for 1h	Amorphous	Oxidation test: 500°C 120h, air	[18]
	M4	47.9	22.81	10.94	3.43	1.48	3.04	10.39		14.7	460	497	14.9	452	495	600°C for 1h	Amorphous	-	
	M5	45.86	24.9	11.8	3.41	1.47	3.03	10.34		14.7	476	488	15	-	475	600°C for 1h	Amorphous	-	
TiO_x $\alpha \approx 7\text{-}9 \cdot 10^{-6}$ °C^{-1}	T1	SiO_2 30.91 Al_2O_3 20.60 TiO_2 20.60 Y_2O_3 15.45 CaO 5.15 K_2O 2.13 Na_2O 5.15							1500°C for 1h + 1550 for 30 minutes, air	8.6	734	792	9.1		1081	1300°C for 10 min+ 855°C for 0.5 h	$Y_2Ti_2O_7$ $CaAl_2Si_2O_8$	Oxidation test: 600°C 120h, air	[20]
p-type																			
HMS $[MnSi_{1.74}]$ $\alpha \approx 11.5 \cdot 10^{-6}$ °C^{-1}	G11	SiO_2 66.3 BaO 15.9 K_2O 9.8 Na_2O 2.7 LiO_2 2.3 Al_2O_3 1.8 B_2O_3 1.2							1450-1500°C for 1h, air	9	500 (DSC)	-	10.7	462	520	700°C for 1h	$Ba_2Si_6O_{16}$ SiO_2 (cristobalite)	Oxidation test: 600° 500hrs, air Cycling test: RT-600°C, 10 cycles, 1h dwell, air	[21]
	Hybrid coating																		
p-type	Acronym	Composition (vol%)											Deposition thermal treatment: temperature (°C), time (h),Ar flow					Oxidation test	Ref
Zn doped THD $[Cu_{11.5}Zn_{0.5}Sb_4S_{13}]$	CP4040 water-based resin	Silicone emulsion 30-50 Zinc oxide < 1 Trizinc bis < 4 Titanium dioxide 1-5 Magnesium Silicate Hydrate 1-5 Mica 5-10 Water 20-30											250°C for 45 minutes					400°C 120h	[19]

3. Results and discussion

3.1 Coating for n-type thermoelectrics

3.1.1 Sb-doped magnesium-based silicide

The *Sb-doped Mg2(Si,Sn)*, with chemical formula $Mg_2Si_{0.487}Sn_{0.5}Sb_{0.013}$, is a n-type TE. XRD analysis (Figure 1a), showed the presence of a single solid solution of Mg_2Si and Mg_2Sn with chemical formula similar to $Mg_2Si_{0.4}Sn_{0.6}$ as the main phase. The oxidation test on the thermoelectric substrate was performed at 500°C with a dwell time of 120 h in air. Five different glass compositions were designed, characterized and tested as potentially oxidation protective coating for $Mg_2Si_{0.487}Sn_{0.5}Sb_{0.013}$ (labelled from M1 to M5 in Table I). As mentioned above, in order to match the CTE of the Sb-doped $Mg_2(Si,Sn)$ of $17.6 \cdot 10^{-6}$ K^{-1} in the temperature range 50-300°C, all the glasses included high contents of alkaline oxides like K_2O and Na_2O, and the addition of MgO to reduce the Mg diffusion from the TE substrate. Additionally, a T_g lower than 500 °C was the target in order to ensure an adequate viscosity of the glass during the coating process that could not exceed 720°C (the TE sintering temperature).

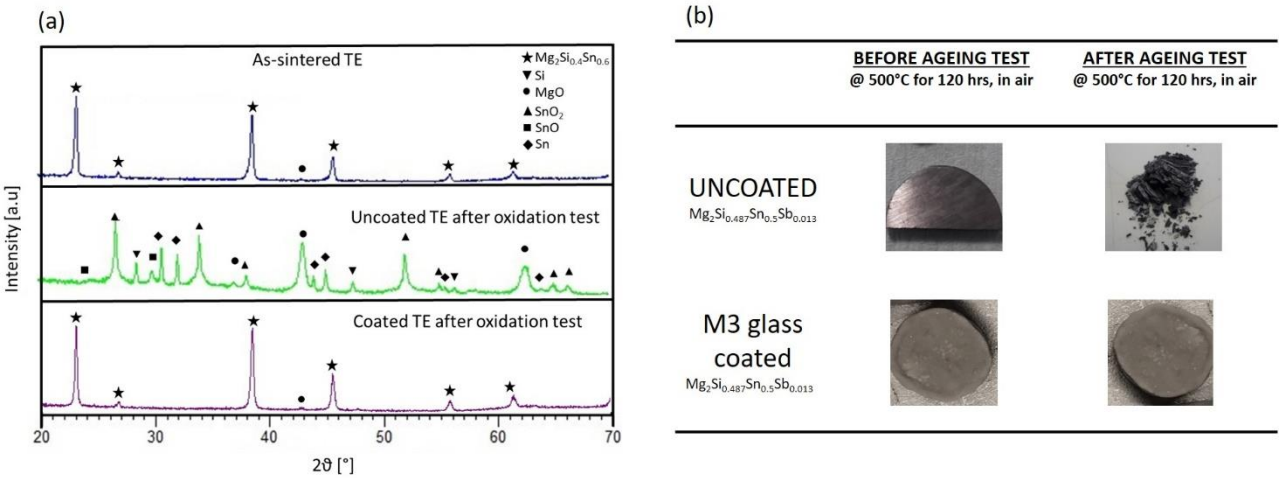

Figure 1. (a) XRD pattern of as-sintered $Mg_2Si_{0.487}Sn_{0.5}Sb_{0.013}$, uncoated and coated $Mg_2Si_{0.487}Sn_{0.5}Sb_{0.013}$after the oxidation test at 500°C for 120 h; (b) macrographs of uncoated $Mg_2Si_{0.487}Sn_{0.5}Sb_{0.013}$ and M3 glass coated $Mg_2Si_{0.487}Sn_{0.5}Sb_{0.013}$ before and after the ageing test at 500 °C for 120 h. The images are adapted from D'Isanto F et al. [18]

The deposition thermal treatment for each composition (Table 1) was selected after evaluation of the sintering and crystallization behavior, with the HSM and DTA, respectively. In order to identify the crystalline phases present in the five compositions, the XRD was carried out on glass pellets obtained after the deposition heat treatment (Figure 2b). In the M1 glass-ceramic after thermal treating at 650°C for 1h, the cubic $Ca_9Al_6O_{18}$ was identified as the main phase and the $KAlSiO_4$ was detected as a secondary phase. Furthermore, an amorphous halo was clearly visible, suggesting the presence of a residual glassy phase. For the M2 glass-ceramic, heat treated under the same conditions, the calcium aluminium oxide was still the main phase, but the intensity of the main peak of the potassium aluminium silicate increases considerably. The amorphous halo related to the residual glassy phase seems to be decreased. No clear evidence of crystalline phases was found for M3 (after sintering at 550°C for 1h), and the M4 and M5 compositions (after the sintering at 600°C for 1h). Dilatometric analyses, carried out on sintered pellets obtained with different deposition heat treatment, are reported in Figure 2a and the values of the CTE are reported in Table I. In the same table, for each glass-based composition, T_g and T_d (dilatometric softening point) are reported before and after the deposition thermal treatment. Since the values of the coefficient of thermal expansion obtained for M1, M2, M4

and M5 after the deposition treatment were too high in comparison with the Sb-doped $Mg_2(Si,Sn)$, these materials were not considered as appropriate coatings for the Mg silicide substrate.

SEM analyses carried out on M3 coated Mg silicide, previously discussed in [18], showed that the coating was well adherent to the substrate, no pores, cracks or delamination phenomena were visible at the coating/TE interface after the deposition treatment. No crystalline phases were found, accordingly to XRD pattern reported in Figure 2b. A good thermo-mechanical compatibility was found between the coating and the thermoelectric substrate. The value of the coefficient of thermal expansion of M3 glass-based coating is ~ $17 \cdot 10^{-6}$ K^{-1} and it is slightly lower than that of the $Mg_2Si_{0.487}Sn_{0.5}Sb_{0.013}$ substrate (17.6·10−6 K−1), which led to a moderate compression state in the coating [4,21], thus making the coated Sb-doped $Mg_2(Si,Sn)$ potentially more resistant to the propagation of cracks during the cooling process or under thermal cycling. Therefore, M3 glass-based coated TE and uncoated samples were subjected to an ageing test at 500°C for 120 h in air. Figure 1b shows samples before and after the oxidation test, and it is clear that the oxidative atmosphere had a strong effect on the uncoated sample. It was completely oxidised and turned into powder, while the coated sample appeared unaffected. Furthermore, the XRD pattern of the aged $Mg_2Si_{0.487}Sn_{0.5}Sb_{0.013}$ for 120 h at 500°C in air without coating (Figure 1a) showed the decomposition of the thermoelectric substrate into a mixture of compounds: MgO, SnO_2, SnO, Sn and Si, as previously reported [18,22]. The XRD pattern of the coated sample after the above-mentioned oxidation test (Figure 1a) is identical with that of the of the as-sintered sample, thus demonstrating the efficacy of the M3 glass-based coating to protect the TE material under oxidative atmosphere at 500°C for 120 h. However, thermoelectric properties of M3 coated samples should be investigated to further validate the effectiveness of the glass-based coating: a reaction could be taken place between the coating and the TE material that cannot be observed by SEM or XRD, but could decrease the TE material performances.

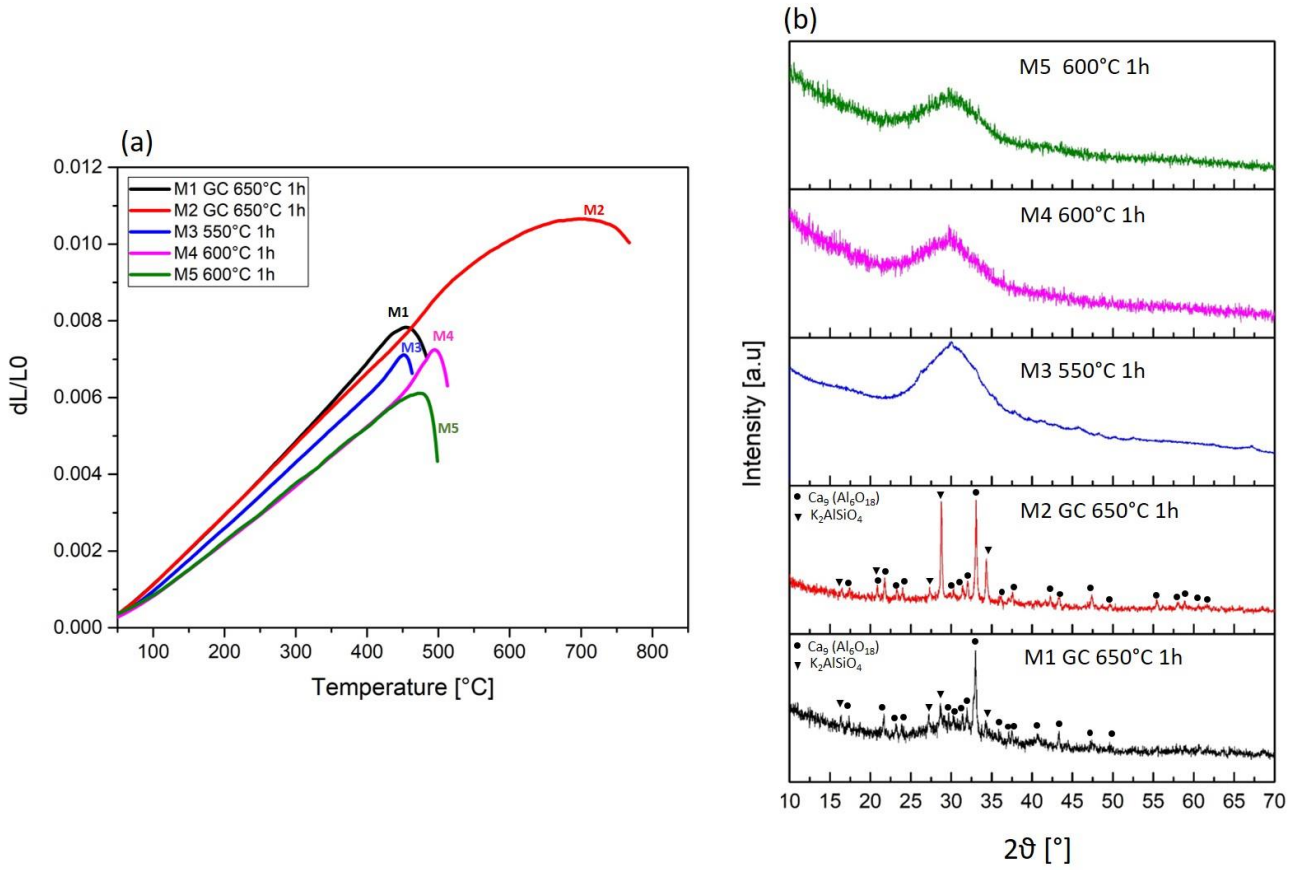

Figure 2. (a) Dilatometry curves and (b) XRD pattern of: M1 and M2 glass-ceramic obtained after deposition heat treatment at 650°C for 1h; M3 glass-based coating obtained after deposition heat treatment at 550°C for 1h; M4 and M5 glass-based coatings obtained after deposition heat treatment at 600°C for 1h.

3.1.2 Titanium suboxide

The second n-type thermoelectric studied was the *titanium suboxide*, TiO_{2-x}. In order to protect this thermoelectric substrate against oxidation up to 600°C, a new silica-based glass labelled as T1 [20], with composition and characteristic temperatures reported in Table I, was produced to match the thermal expansion coefficient of titanium suboxide that is ~ 7-9 $\cdot 10^{-6}$ K^{-1} [23]. The microstructure of as-cast T1, which is described in [20], showed the detection of two different phases: brighter uniformly-dispersed round-shaped grains of a size ranging from 200 to 250 nm immersed in a continuous dark matrix. Different hypotheses were considered to explain the development of this microstructure, however XRD and TEM/SAED analyses (Figure 3a) supported the hypothesis of the presence of a glass-phase separation, which caused the formation of glass droplets in which

primary $Y_2Ti_2O_7$ crystals formed. $Y_2Ti_2O_7$ has a coefficient of thermal expansion of ~$8.4 \cdot 10^{-6} K^{-1}$ in the 300–1000°C range [24], a value that is similar to that of titanium suboxide ($7–9 \cdot 10^{-6} K^{-1}$) [23]. Furthermore, $Y_2Ti_2O_7$ pyrochlore is chemically stable at high temperatures, has a low thermal conductivity (in the range of 2.25–2.6 W $m^{-1} K^{-1}$) [24] and, consequently, is a promising candidate material for the oxidation protection of TiO_{2-x}. Considering the DTA and HSM analyses of the T1 glass, the coating deposition heat-treatment was chosen as 1300°C for 10 min, followed by a heat-treatment at 855°C for 30 min As reported in [20] and in Table I, the coefficient of thermal expansion of the T1 parent glass is $8.6 \cdot 10^{-6} K^{-1}$ between 200 °C and 500 °C, while the dilatometric softening point is 792 °C (Figure 3c-1). The heat treatment necessary to consolidate the coating process determined a slight increase of the CTE of the T1 parent glass, anyway the CTE value of the T1 glass-ceramic is still compatible ($9.1 \cdot 10^{-6} K^{-1}$) with the titanium suboxide substrate. The most interesting result is that the sinter-crystallization heat treatment led to higher characteristic T (i. e. the dilatometric softening temperature, indicated as T_d in Figure 3c, increased significantly from 792°C for the parent glass, to 1081°C for the glass-ceramic in Figure 3c-2), thus increasing and extending the working temperature of the T1 system.

A further examination of the glass-ceramic microstructure was carried out by means TEM and SAED analyses (Figure 3b). The diffraction patterns of the black crystals confirmed that they are the cubic $Y_2Ti_2O_7$ phase, while the light-grey crystals are the triclinic $CaAl_2Si_2O_8$ phase. Furthermore, it can be seen, at higher magnifications (green circle in Figure 3b), that there are very small particles in some regions of the light amorphous area; the SAED analysis confirmed that these particles are hexagonal phase Y_2TiO_5 in an amorphous matrix.

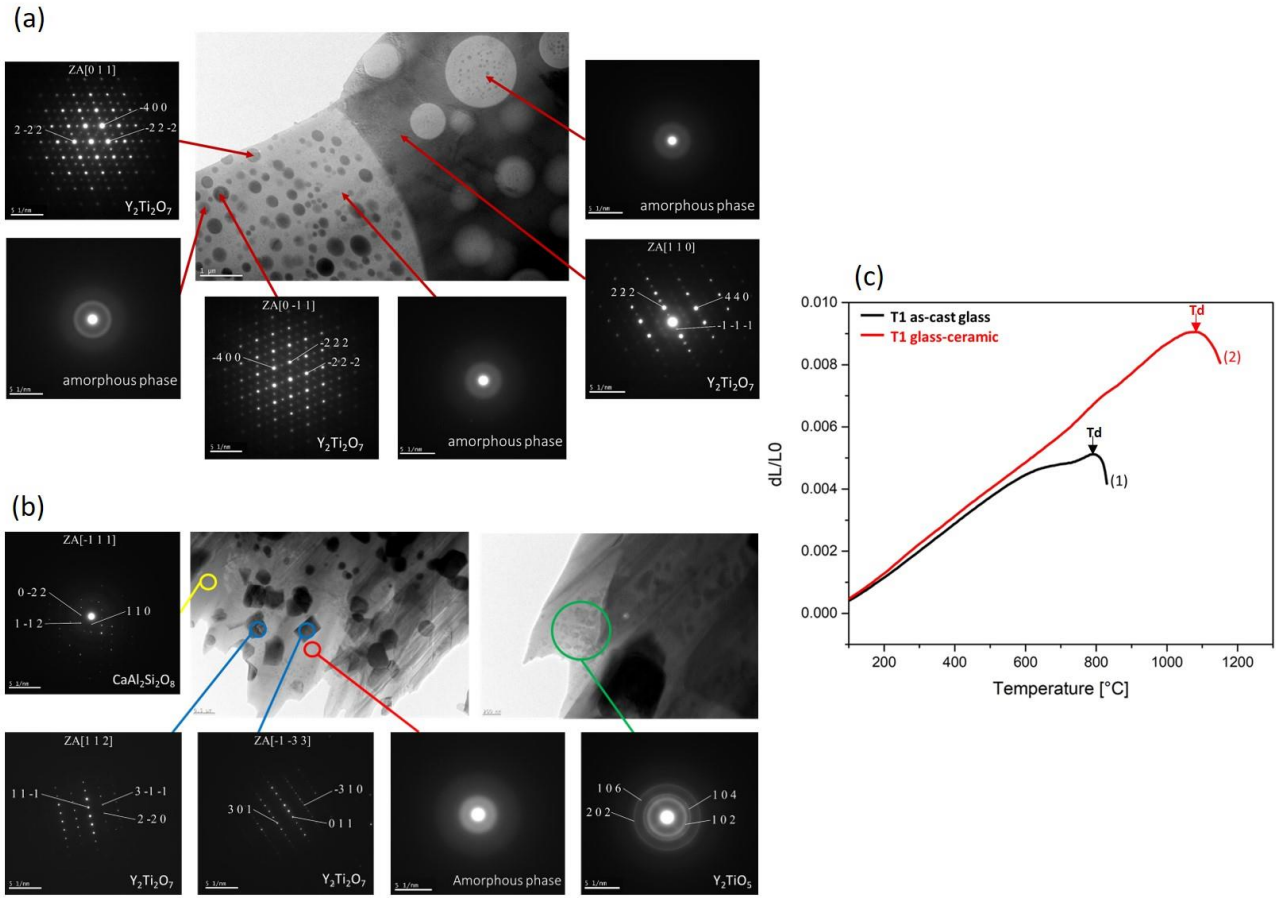

Figure 3. TEM and SAED analyses of (a) as-cast T1 glass and (b) T1 glass-ceramic; dilatometry curves of (c-1) as-cast T1 glass and (c-2) T1 glass-ceramic. The images are adapted (Figure 3 a,b) and reprinted (Figure 3c) from D'Isanto F. et al. [20]

Based on the above results, the T1 glass-ceramic coated TiO_{2-x} and uncoated samples were submitted to a preliminary oxidation test at 600 °C for 120 h in air. Figure 4a shows the cross-section of a coated sample after the oxidation test. The formation of cracks due to thermal stresses was not observed and the microstructure of the glass-ceramic was not affected by the heat treatment as compared with that showed before oxidation test [20]; the T1 glass-ceramic has a glass transition temperature >750 °C (as shown in Figure 3c) and below the T_g, the glass viscosity is so high that structural rearrangements required for crystal nucleation and growth are unlikely to occur [25]. Furthermore, the ≈ 1.5 µm thick reaction layer visible at the T1/TiO_{2-x} interface after the oxidation test (Figure 4a) is unchanged if compared with that shown in SEM images before the test [20], and the excellent adhesion of the coating to the thermoelectric material is maintained, even after the exposure to severe conditions. The

XRD pattern of the uncoated substrate following the oxidation test (Figure 4b) shows that it completely oxidised to TiO_2. On the contrary, it is encouraging to observe that the XRD pattern of the coated sample after the oxidation test (after removing the outer layers to reveal pristine TiO_{2-x}), is quite similar to that of the as-sintered sample. The comparison of the two diffractograms, shows some differences concerning the $Ti_{10}O_{18}$ phase, represented by peaks with different relative ratios in the two samples. This is particularly evident in the 50-60° 2ϑ range of Figure 4b. These changes could be due to XRD analyses carried out on bulk samples that may be cause a variation in the intensity peaks. On the other hand, they could indicate an oxygen very slow migration through T1 glass-ceramic coating leading to an increment in $Ti_{10}O_{18}$ crystalline phase. In order to evaluate if the results obtained with XRD analysis was related to a very long-term failure mode or if the T1 glass-ceramic was effective in protecting the TiO_{2-x} substrate up to 600°C for 120 h in air, transport properties need to be measured. They will be performed to confirm the efficacy of the T1 glass-ceramic coating to exclude degradation of the thermoelectric material which can lead to reduce the reliability of thermoelectric components.

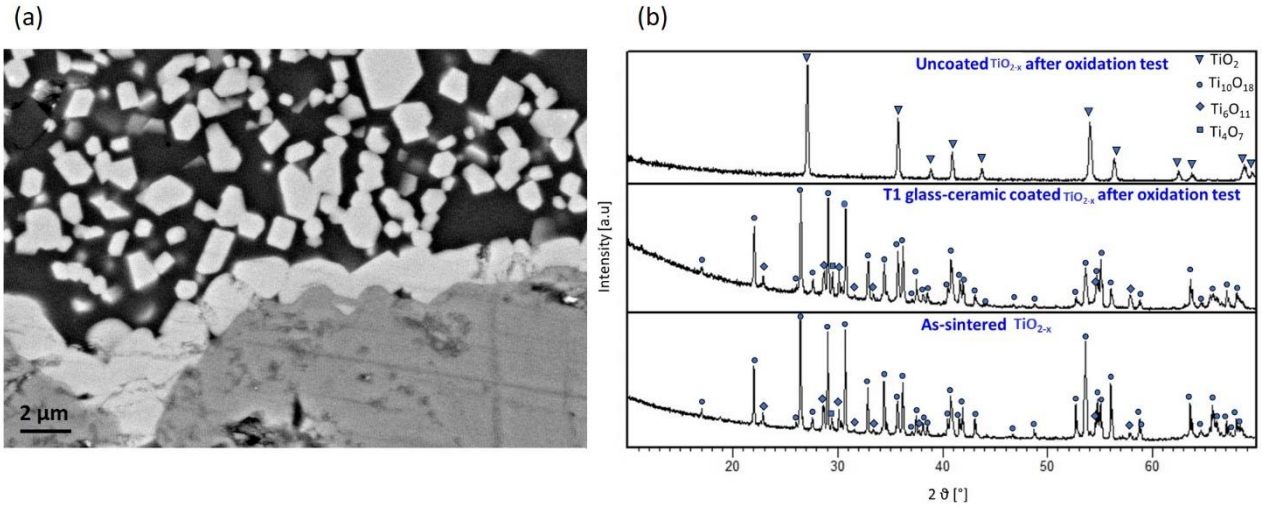

Figure 4. (a) SEM image (BSE) of the cross-section of a T1 glass-ceramic coated TiO_{2-x} after the oxidation test at 600°C for 120 h; (b) XRD pattern of uncoated TiO_{2-x}, T1 glass-ceramic coated TiO_{2-x} and as-sintered TiO_{2-x}. The images are adapted from D'Isanto F et al. [20]

3.2 Coating for p-type thermoelectrics

3.2.1 Higher manganese silicide

Higher manganese silicide (HMS), $MnSi_{1.74}$, is a p-type thermoelectric. The XRD analysis of as-sintered HMS (Figure 5e) showed that the main phase is $Mn_{27}Si_{47}$ and that MnSi is present in very small amounts. The glass used to protect HMS against oxidation, labelled G11, was previously designed by F. Smeacetto et al.[26]; its composition is presented Table I. It is a lead-free glass with characteristic temperatures suitable to be applied by slurry deposition and direct heating on the HMS substrate, without exceeding the sintering temperature of the TE substrate (720 °C). The glass-ceramic, obtained from the heat treatment of the G11 glass, was chosen as coating for higher manganese silicide because of its thermo-mechanical properties. After the coating deposition, a heat treatment carried out at 700 °C for 1h under flowing Ar. The G11 glass-ceramic system showed a coefficient of thermal expansion of $10.7 \cdot 10^{-6}$ K^{-1}, 200-400°C, which matches well with this type of silicide ($11.5 \cdot 10^{-6}$ K^{-1}, from room temperature to 700°C), with a softening point around 520 °C and a significant amount of residual amorphous phase [4]. For this reason, the self- healing properties of G11 glass-ceramic were evaluated by manually engraving a scratch on its surface with a diamond tip (Figure 5a) and introducing several indentations on the glass-ceramic coating (Figure 5c). All of the cracks were healed and indentation marks were not visible (Figures 5b and 5d) after heating at 600°C for 30 min, under flowing Ar.

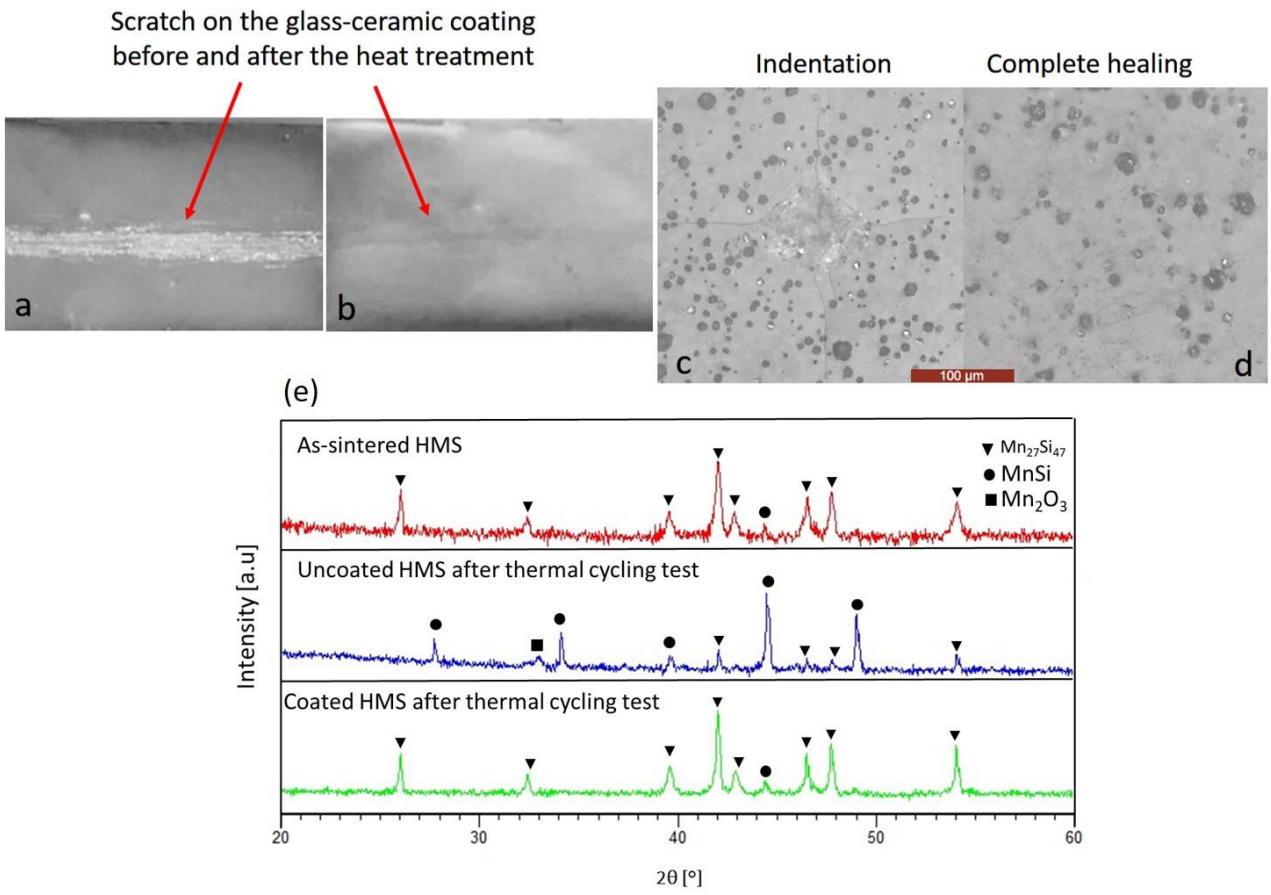

Figure 5. (a,b) Healing of a scratch in the glass-ceramic coating and (c,d) of indentation mark and cracks, after heat treatment at 600°C, for 30 minutes, under Ar flow ; (e) XRD pattern of as-sintered HMS, uncoated and coated HMS after thermal cycling from room temperature to 600°C, dwelling time 1h, for 10 cycles. The images are reprinted (Figure 3a-d) and adapted (Figure 5e) from D'Isanto F. et al. [21]

The need for effective protection in oxidative atmosphere was demonstrated by SEM characterisation and XRD analysis of uncoated HMS after thermal ageing at 600°C for 500 h and thermal cycling from room temperature to 600°C, with a dwell time 1h, for 10 cycles, in air (Figure 5e) [4,21]. The formation of an incoherent silica scale on the whole surface of the thermoelectric, due to the reaction between the HMS and oxygen, caused the formation of a Si-deficient layer (MnSi), as shown by the XRD pattern in Figure 5e.

On the contrary, from the XRD analyses of the coated HMS, no evidence was found of the formation of the MnSi layer at the coating/HMS interface after the thermal cycling (Figure 5e) and thermal

ageing in the same above-mentioned conditions. Furthermore, the G11 glass-ceramic oxidation protective coating effectiveness is demonstrated by the thermoelectric properties reported in Figure 6, which show the temperature dependence of the power factor and zT of the as-sintered HMS, coated and uncoated HMS after thermal cycling from room temperature to 600°C, dwell time 1h, for 10 cycles.

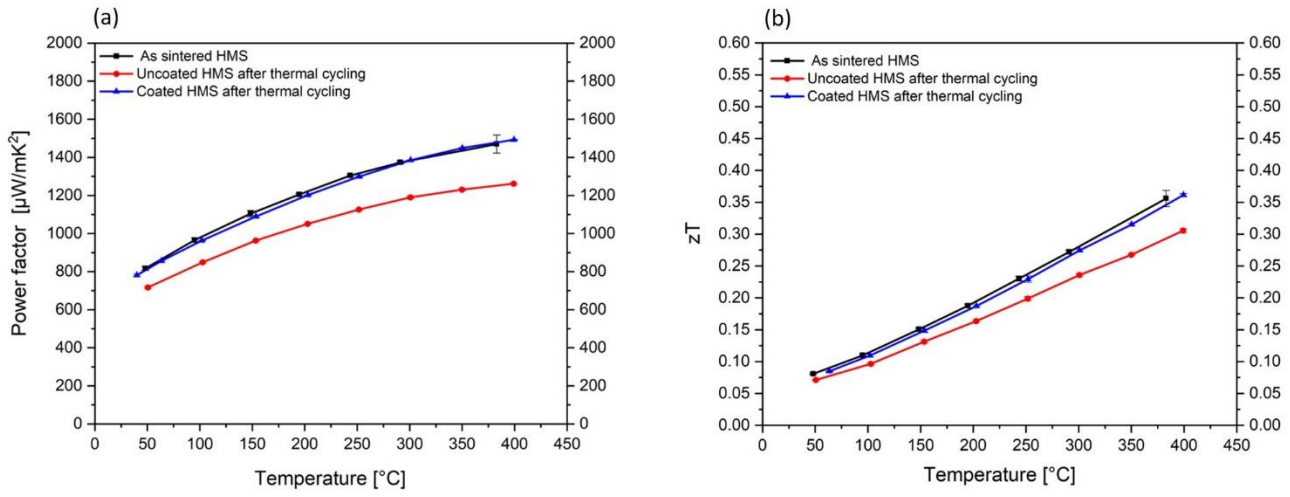

Figure 6. Temperature dependence of (a) Power factor and (b) zT of the as sintered HMS, coated and uncoated HMS after thermal cycling from room temperature to 600°C, dwelling time 1h, for 10 cycles. The images are adapted from D'Isanto F et al. [21].

Figure 6 shows the beneficial effect of the coating in these operative conditions. It can be noticed that the coating allowed the differences in the power factor values of the as-sintered and coated samples to be maintained within the error bars, avoiding a decrease observed in the uncoated specimen (Figure 6a). Furthermore, the coating avoided the increase of the electrical resistivity measured in the uncoated sample after the oxidation treatment if compared to the as-sintered specimen[21]. Regarding the figure of merit zT (Figure 6b), it can be observed that the coated HMS shows an almost unchanged zT compared to the as-sintered specimen; both samples show higher values than those of the uncoated TE, with differences that increase with increasing temperature. It can therefore be assumed that the glass-ceramic coating provided effective protection, thus preventing the oxidation of HMS under these thermal cycling conditions. The integrity of the coating and the soundness of the interface

confirmed the excellent CTE matching between HMS and coating, which prevented the formation of deleterious residual stresses within the coated sample [21].

3.2.2 Zn-doped Tetrahedrite

The second p-type TE substrate was the *Zn-doped Tetrahedrite* with chemical formula $Cu_{11.5}Zn_{0.5}Sb_4S_{13}$. Since glass and glass-ceramic coatings would require a deposition temperature too high for THD, a commercial hybrid resin with low curing temperature and with nominal temperature resistance up to 590°C, was employed as a protective resistance coating. The effectiveness of the coating in avoiding oxidation of tetrahedrite was demonstrated by assessing the electrical properties of both the uncoated and coated THD before and after oxidation test at 400°C for 120h in air. XRD analysis of an uncoated sample after ageing at 400°C (Figure 7b) showed the presence of orthorhombic antimony oxides Sb_2O_3 and Sb_2O_4, with $Cu_{12}Sb_4S_{13}$, Cu_2S and CuS as secondary phases.

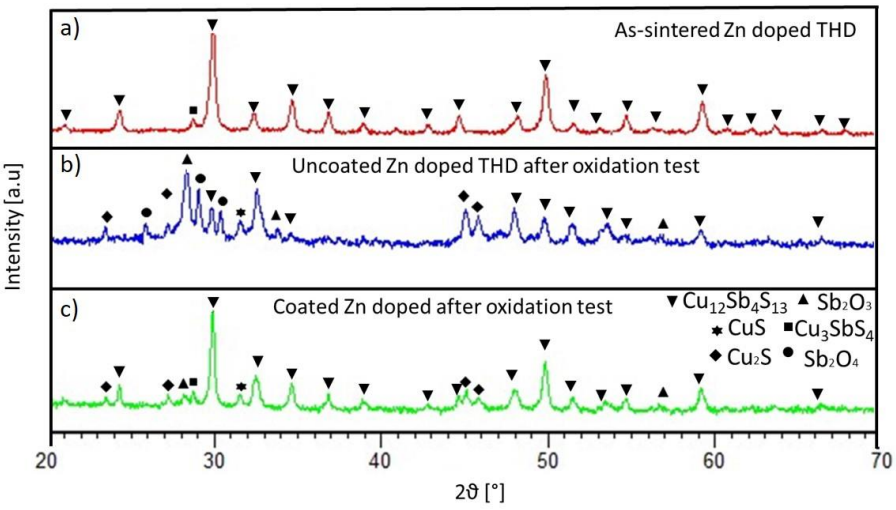

Figure 7. XRD pattern of (a) as-sintered Zn doped THD, (b) uncoated and (c) coated Zn doped THD, after the oxidation test at 400°C for 120 h.

On the other hand, XRD analysis of the coated THD after oxidation test at 400°C for 120h (Figure 7c) showed that the main phase remained the $Cu_{12}Sb_4S_{13}$ with Cu_3SbS_4 as a secondary phase (as for the sample before the oxidation test, Figure 7a), and the presence of oxidation layers of antimony

oxide (Sb_2O_3) with traces of Cu_2S and CuS. Figure 8 shows the results obtained from thermoelectric measurements (electrical resistivity, Seebeck and power factor) carried out on as-prepared, uncoated and coated samples after oxidation testing, suggesting that the formation of secondary phases in the uncoated sample observed in XRD analyses (Figure 7b) reduced the carrier concentration, and therefore led to a higher resistivity (Figure 8a). Seebeck coefficients of the aged Zn doped THD without coating (Figure 8b), were slightly lower than those as-sintered and with coating, which did not show any differences. On the other side, the coating was able to avoid the increase in electrical resistivity observed for the uncoated sample. Consequently, the Seebeck coefficient and the power factor of the uncoated sample decreased, while the coated sample maintained similar values to as-sintered one (Figure 8b-c). No Figur of merit data (zT) were reported for this thermoelectric substrate, because thermal conductivity has not measured yet.

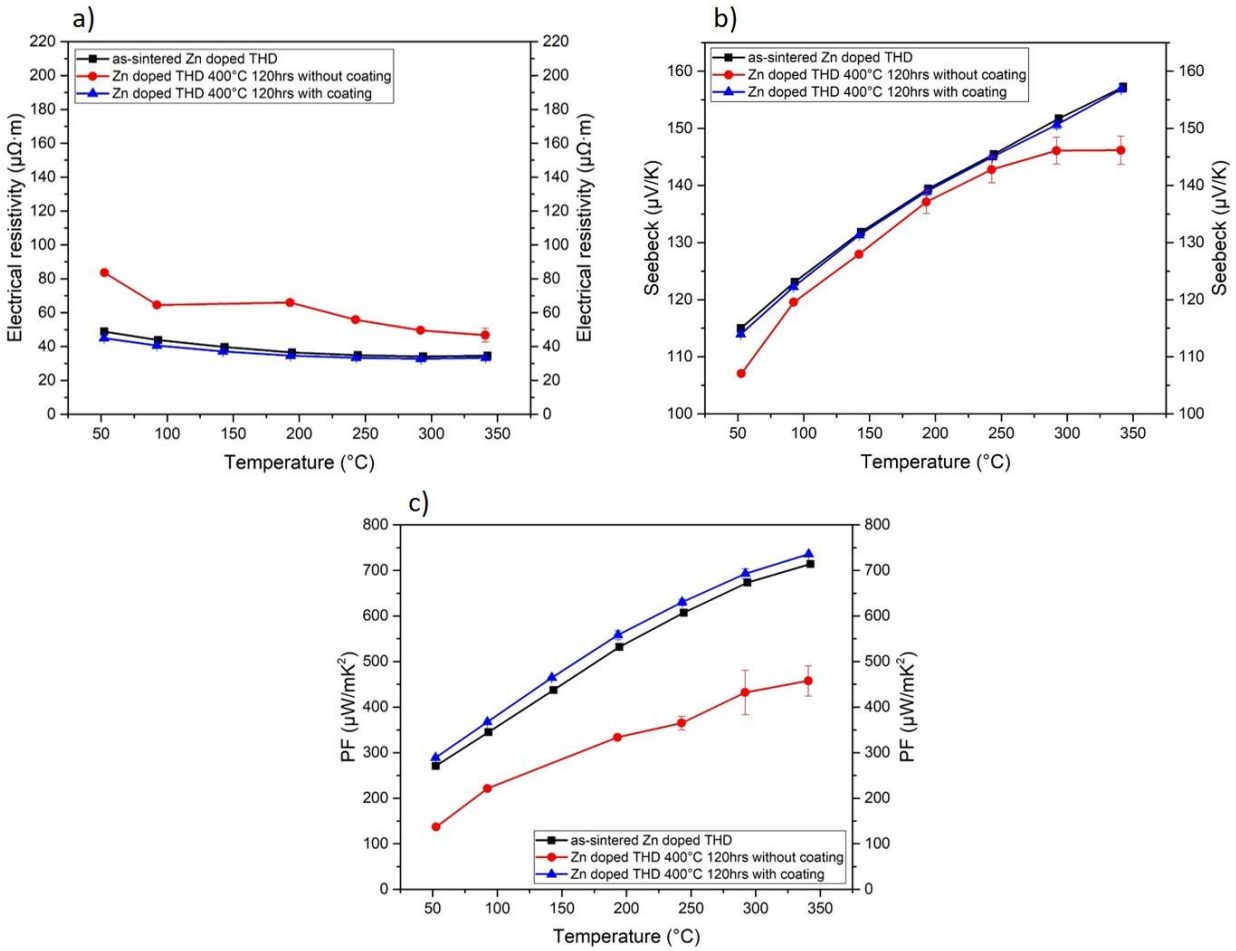

Figure 8. Temperature dependence of the (a) electrical resistivity, (b) Seebeck coefficient, (c) power factor of the as-sintered Zn doped THD, uncoated and coated Zn doped THD, after the oxidation test at 400°C for 120h.

4. Conclusions

In this paper, the results concerning new oxidation protective coatings for four different thermoelectric materials (2 n-type and 2 p-type) were reviewed and discussed in terms of their thermal characterisation, their thermo-mechanical compatibility with the substrates as well as their efficiency in different relevant conditions (thermal ageing or thermal cycling). The design and the development of new glass and glass-ceramics as promising oxidation protective coatings were the main focus of this paper. Slurry deposition of the coatings is an easy efficient method to overcome the main drawback of oxidation and could extend the temperature range for thermoelectric applications. Furthermore, the effectiveness of a hybrid commercial coating in as a novel and easy approach to coat TE substrates in order to avoid their decomposition when they cannot be heated at a temperature higher than 400°C (sintering temperature), was successfully demonstrated in this temperature range.

This study has identified some thermoelectric substrates degradation issues and provided a comprehensive overview of different glass-based systems and processing to assess their functionality in protecting TE substrates devices at T higher than 400°C, thus potentially extending their efficiency. The preliminary ageing/ thermal cycling reported in this work (short time of testing) suggest that these coatings are promising candidate for protecting thermoelectrics, but longer tests in more severe conditions and missing thermoelectric and transport properties will be perform to further validate the efficacy of oxidative protective coatings proposed.

This paper represents a valuable contribution to the integration of advanced engineering ceramics for energy conversion systems and the research findings have important implications for developing of durable and reliable TE modules.

Declaration of competing interest

The authors declare that they have no known competing financial interests or personal relationships that could have appeared to influence the work reported in this paper.

References

[1] A. Zecca, L. Chiari, Fossil-fuel constraints on global warming, Energy Policy. 38 (2010) 1–3. https://doi.org/10.1016/j.enpol.2009.06.068.

[2] J. He, T.M. Tritt, Advances in thermoelectric materials research: Looking back and moving forward, Science (80-.). 357 (2017). https://doi.org/10.1126/science.aak9997.

[3] J.J. Gutiérrez Moreno, J. Cao, M. Fronzi, M.H.N. Assadi, A review of recent progress in thermoelectric materials through computational methods, Mater. Renew. Sustain. Energy. 9 (2020) 1–22. https://doi.org/10.1007/s40243-020-00175-5.

[4] H. Ning, M.J. Reece, F. Smeacetto, M. Salvo, Oxidation protective glass–ceramic coating for higher manganese silicide thermoelectrics, J. Mater. Sci. 51 (2016) 9484–9489. https://doi.org/10.1007/s10853-016-0192-1.

[5] A. de P. Shyikira, N. Akhtar, G. Skomedal, T.O. Sætre, P.H. Middleton, High temperature oxidation of higher manganese silicides, Corros. Sci. 185 (2021) 109327. https://doi.org/10.1016/j.corsci.2021.109327.

[6] M. Kambe, T. Jinushi, Z. Ishijima, Encapsulated Thermoelectric Modules and Compliant Pads for Advanced Thermoelectric Systems, J. Electron. Mater. 39 (2010) 1418–1421. https://doi.org/10.1007/s11664-010-1315-0.

[7] J.R. Salvador, J.Y. Cho, Z. Ye, J.E. Moczygemba, A.J. Thompson, J.W. Sharp, J.D. König,

R. Maloney, T. Thompson, J. Sakamoto, H. Wang, A.A. Wereszczak, G.P. Meisner, Thermal to Electrical Energy Conversion of Skutterudite-Based Thermoelectric Modules, J. Electron. Mater. 42 (2013) 1389–1399. https://doi.org/10.1007/s11664-012-2261-9.

[8] G.J.S. J. Sakamoto, T. Caillat, J.-P. Fleurial, Method of suppressing sublimation in advanced thermoelectric devices, U.S. Patent No. 7480984 B1, 2009.

[9] M.S. El-Genk, H.H. Saber, T. Caillat, J. Sakamoto, Tests results and performance comparisons of coated and un-coated skutterudite based segmented unicouples, Energy Convers. Manag. 47 (2006) 174–200. https://doi.org/10.1016/j.enconman.2005.03.023.

[10] H.H. Saber, M.S. El-Genk, T. Caillat, Tests results of skutterudite based thermoelectric unicouples, Energy Convers. Manag. 48 (2007) 555–567. https://doi.org/10.1016/j.enconman.2006.06.008.

[11] G.S. J. Sakamoto, T. Calliat, J. Fleurial, Coating Thermoelectric Devices to Suppress Sublimation, NASA's Jet Propulsion Laboratory, NASA Tech Briefs. (2007) 5–6.

[12] H.H. Saber, M.S. El-Genk, Effects of metallic coatings on the performance of skutterudite-based segmented unicouples, Energy Convers. Manag. 48 (2007) 1383–1400. https://doi.org/10.1016/j.enconman.2006.04.024.

[13] D. Crane, Thermoelectric Waste Heat Recovery Program for Passenger Vehicles, US Dep. Energy Effic. Renew. Energy. (2012). http://energy.gov/sites/prod/files/2014/07/f17/ace080_barnhart_2014_o.pdf.

[14] F. D'Isanto, New oxidation protective coatings for thermoelectric materials, 2020.

[15] Y.S. Park, T. Thompson, Y. Kim, J.R. Salvador, J.S. Sakamoto, Protective enamel coating for n- and p-type skutterudite thermoelectric materials, J. Mater. Sci. 50 (2015) 1500–1512. https://doi.org/10.1007/s10853-014-8711-4.

[16] K. Zawadzka, E. Godlewska, K. Mars, M. Nocun, A. Kryshtal, A. Czyrska-Filemonowicz,

Enhancement of oxidation resistance of CoSb3thermoelectric material by glass coating, Mater. Des. 119 (2017) 65–75. https://doi.org/10.1016/j.matdes.2017.01.055.

[17] H. Dong, X. Li, X. Huang, Y. Zhou, W. Jiang, L. Chen, Improved oxidation resistance of thermoelectric skutterudites coated with composite glass, Ceram. Int. 39 (2013) 4551–4557. https://doi.org/10.1016/j.ceramint.2012.11.051.

[18] F. D'Isanto, F. Smeacetto, M.J. Reece, K. Chen, M. Salvo, Oxidation protective glass coating for magnesium silicide based thermoelectrics, Ceram. Int. 46 (2020) 24312–24317. https://doi.org/10.1016/j.ceramint.2020.06.212.

[19] F. Gucci, F. D'Isanto, R. Zhang, M. Reece, F. Smeacetto, M. Salvo, Oxidation Protective Hybrid Coating for Thermoelectric Materials, Materials (Basel). 12 (2019) 573. https://doi.org/10.3390/ma12040573.

[20] F. D'Isanto, F. Smeacetto, H.P. Martin, R. Sedlák, M. Lisnichuk, A. Chrysanthou, M. Salvo, Development and characterisation of a Y2Ti2O7-based glass-ceramic as a potential oxidation protective coating for titanium suboxide (TiOx), Ceram. Int. 47 (2021) 19774–19783. https://doi.org/10.1016/j.ceramint.2021.03.316.

[21] M. Salvo, F. Smeacetto, F. D'Isanto, G. Viola, P. Demitri, F. Gucci, M.J. Reece, Glass-ceramic oxidation protection of higher manganese silicide thermoelectrics, J. Eur. Ceram. Soc. 39 (2019) 66–71. https://doi.org/10.1016/j.jeurceramsoc.2018.01.007.

[22] G. Skomedal, A. Burkov, A. Samunin, R. Haugsrud, H. Middleton, High temperature oxidation of Mg 2 (Si-Sn), Corros. Sci. 111 (2016) 325–333. https://doi.org/10.1016/j.corsci.2016.05.016.

[23] J.K. Gill, O.P. Pandey, K. Singh, Role of sintering temperature on thermal, electrical and structural properties of Y2Ti2O7 pyrochlores, Int. J. Hydrogen Energy. 36 (2011) 14943–14947. https://doi.org/10.1016/j.ijhydene.2011.02.138.

[24] S.T. Nguyen, T. Nakayama, H. Suematsu, T. Suzuki, M. Takeda, K. Niihara, Low thermal conductivity Y2Ti2O7 as a candidate material for thermal/environmental barrier coatings, Ceram. Int. 42 (2016) 11314–11323. https://doi.org/https://doi.org/10.1016/j.ceramint.2016.04.052.

[25] V.M. Fokin, E.D. Zanotto, N.S. Yuritsyn, J.W.P. Schmelzer, Homogeneous crystal nucleation in silicate glasses: A 40 years perspective, J. Non. Cryst. Solids. 352 (2006) 2681–2714. https://doi.org/10.1016/j.jnoncrysol.2006.02.074.

[26] F. Smeacetto, M. Salvo, A. Ventrella, S. Rizzo, M. Ferraris, Durable Glass-Ceramic Coatings for Foam Glass, Int. J. Appl. Glas. Sci. 3 (2012) 69–74. https://doi.org/10.1111/j.2041-1294.2011.00071.x.

Table caption

Table I. Summary of glass-based oxidation protective coatings for Sb doped $Mg_2(Si,Sn)$, TiO_{2-x} and HMS thermoelectrics: composition, thermal and thermo-mechanical properties, main crystalline phases, deposition thermal treatment, oxidation/cycling test parameters. Composition and heat-treatment of a commercial hybrid resin used to protect Zn-doped THD are also illustrated.

Figure captions

Figure 1. (a) XRD pattern of as-sintered $Mg_2Si_{0.487}Sn_{0.5}Sb_{0.013}$, uncoated and coated $Mg_2Si_{0.487}Sn_{0.5}Sb_{0.013}$after the oxidation test at 500°C for 120 h; (b) macrographs of uncoated $Mg_2Si_{0.487}Sn_{0.5}Sb_{0.013}$ and M3 glass coated $Mg_2Si_{0.487}Sn_{0.5}Sb_{0.013}$ before and after the ageing test at 500 °C for 120 h. The images are adapted from D'Isanto F et al. [18].

Figure 2. (a) Dilatometry curves and (b) XRD pattern of: M1, M2 glass-ceramic obtained after deposition heat treatment at 650°C for 1h; M3 glass-based coating obtained after deposition heat

treatment at 550°C for 1h; M4, M5 glass-based coatings obtained after deposition heat treatment at 600°C for 1h.

Figure 3. TEM and SAED analyses of (a) as-cast T1 glass and (b) T1 glass-ceramic; dilatometry curves of (c-1) as-cast T1 glass and (c-2) T1 glass-ceramic. The images are adapted (Figure 3 a,b) and reprinted (Figure 3c) from D'Isanto F. et al. [20].

Figure 4. (a) SEM image (BSE) of the cross-section of a T1 glass-ceramic coated TiO_{2-x} after the oxidation test at 600°C for 120 h; (b) XRD pattern of uncoated TiO_{2-x}, T1 glass-ceramic coated TiO_{2-x} and as-sintered TiO_{2-x}. The images are adapted from D'Isanto F et al. [20].

Figure 5. (a,b) Healing of a scratch in the glass-ceramic coating and (c,d) of indentation mark and cracks, after heat treatment at 600°C, for 30 minutes, under Ar flow ; (e) XRD pattern of as-sintered HMS, uncoated and coated HMS after thermal cycling from room temperature to 600°C, dwelling time 1h, for 10 cycles. The images are reprinted (Figure 3a-d) and adapted (Figure 5e) from Salvo M. et al. [21].

Figure 6. Temperature dependence of (a) Power factor and (b) zT of the as sintered HMS, coated and uncoated HMS after thermal cycling from room temperature to 600°C, dwelling time 1h, for 10 cycles. The images are adapted from D'Isanto F et al. [21].

Figure 7. XRD pattern of as-sintered Zn doped THD, uncoated and coated Zn doped THD, after the oxidation test at 400°C for 120 h.

Figure 8. Temperature dependence of the (a) electrical resistivity, (b) Seebeck coefficient, (c) power factor of the as-sintered Zn doped THD, uncoated and coated Zn doped THD, after the oxidation test at 400°C for 120h.